OPEN ACCESS Freely available online

PLOS ONE

Flow and Heat Transfer in Sisko Fluid with Convective Boundary Condition

Rabia Malik*, Masood Khan, Asif Munir, Waqar Azeem Khan

Department of Mathematics, Quaid-i-Azam University, Islamabad, Pakistan

Abstract

In this article, we have studied the flow and heat transfer in Sisko fluid with convective boundary condition over a non-isothermal stretching sheet. The flow is influenced by non-linearly stretching sheet in the presence of a uniform transverse magnetic field. The partial differential equations governing the problem have been reduced by similarity transformations into the ordinary differential equations. The transformed coupled ordinary differential equations are then solved analytically by using the homotopy analysis method (HAM) and numerically by the shooting method. Effects of different parameters like power-law index n, magnetic parameter M, stretching parameter s, generalized Prandtl number Pr and generalized Biot number γ are presented graphically. It is found that temperature profile increases with the increasing value of M and γ whereas it decreases for Pr. Numerical values of the skin-friction coefficient and local Nusselt number are tabulated at various physical situations. In addition, a comparison between the HAM and exact solutions is also made as a special case and excellent agreement between results enhance a confidence in the HAM results.

Citation: Malik R, Khan M, Munir A, Khan WA (2014) Flow and Heat Transfer in Sisko Fluid with Convective Boundary Condition. PLoS ONE 9(10): e107989. doi:10.1371/journal.pone.0107989

Editor: Zhonghao Rao, China University of Mining and Technology, China

Received April 24, 2014; **Accepted** August 20, 2014; **Published** October 6, 2014

Data Availability: The authors confirm that all data underlying the findings are fully available without restriction. All relevant data are within the paper.

Funding: The authors have no support or funding to report.

Competing Interests: The authors have declared that no competing interests exist.

* Email: rabiamalik.qau@gmail.com

Introduction

Because of the occurrence in a variety of engineering operations the boundary layer flow and heat transfer over a stretching surface has gained much importance. A few applications in the field of chemical engineering and metallurgy include extrusion of polymers, production of paper and so forth. The final product's quality massively depends on heat transfer rate between the fluid and stretching surface during the operation of heating and/or cooling. Consequently, most suitable heating and/or cooling fluid must be chosen as it has immense influence on the heat transfer rate. The physical importance of heat transfer over a moving surface has compelled many researchers to report their findings on this topic [1–10].

The convective heat transfer is of excessive significance in procedures in which high temperatures are involved. For instance, gas turbines, nuclear plants, storage of thermal energy etc. Referring to numerous industrial and engineering processes the convective boundary conditions are more practical including material drying, transpiration cooling process etc. Due to the practical importance of convective boundary conditions several researchers have studied and reported results on this topic for viscous fluid. Bataller [11] investigated the Blasius and Sakiadis flows in a viscous fluid with convective boundary conditions. The heat transfer of a viscous fluid over a stretching/shrinking sheet with convective boundary conditions has been studied by Yao *et al.* [12]. Hammad *et al.* [13] discussed the radiation effects and effects of the thermal convective boundary condition, variable viscosity and thermal conductivity on coupled heat and mass transfer with mixed convection. Vajravelu *et al.* [14] presented solution to the unsteady convective boundary layer flow of a viscous fluid over a vertical stretching surface with thermal radiation.

On the other hand, the study of non-Newtonian fluids including Generalized Newtonian Liquid (abbreviated as GNL) with heat transfer has gained extensive importance due to a number of industrial applications such as molten plastic, polymer solutions, pulp and foods etc. At the same time, heat transfer in non-Newtonian fluids with convective boundary conditions has been dealt by a few researchers. The three-dimensional flow of a Jeffrey fluid over a stretching surface with convective boundary conditions has been examined by Hayat *et al.* [15]. In another paper, the flow and heat transfer in an upper-convected Maxwell fluid over a moving surface in the presence of a free stream velocity with convective boundary conditions is studied by Hayat *et al.* [16]. The steady flow and heat transfer in an Eyring Powell fluid over a plate moving continuously concerning convective boundary conditions is also examined by Hayat *et al.* [17]. Srinivas *et al.* [18] examined the influence of chemical reaction and Soret effects on hydromagnetic viscous pulsating flow in a porous channel with convective boundary conditions. Makinde [19] analyzed the thermal stability of viscous fluid flowing steadily through a channel filled with the saturated porous medium. The Sisko model [20,21] a special case of GNL which predicts dilatant and pseudoplastic nature of fluid is not given due attention. It is worth pointing out that a few recent investigations on flow of Sisko fluid with heat transfer have been studied by Khan and Farooq [22] and Khan *et al.* [23,24].

However we can notice that the Sisko fluid with heat transfer analysis specially with an emphasis of convective boundary

conditions is less explored. In the work under consideration we explored the flow and heat transfer in Sisko fluid over a nonlinearly stretching surface with convective boundary condition. It is hoped that present work serves as stimulus for the shear thinning and thickening fluid flows in the areas where high rate of heat transfer or rate of cooling is required such as extrusion processes, glass fiber and storage of thermal energy.

Mathematical Formulation

Flow equations

Let us consider steady, laminar and incompressible flow of Sisko fluid over an isothermal flat sheet (as shown in figure 1). The sheet is stretching with velocity $U(x)=cx^s$, where c and s are non-negative real numbers and the velocity for two-dimensional flow is assumed of the form $\mathbf{V}=[u(x,y),v(x,y),0]$, where (x,y) denotes the Cartesian coordinates. A uniform transverse magnetic field $\mathbf{B}=[0,B_0,0]$ is applied under the assumption of very small magnetic Reynolds number. The governing equations for two-dimensional boundary layer flow are (see ref. [20] for details)

$$\frac{\partial u}{\partial x}+\frac{\partial v}{\partial y}=0, \tag{1}$$

$$u\frac{\partial u}{\partial x}+v\frac{\partial u}{\partial y}=\frac{a}{\rho}\frac{\partial^2 u}{\partial y^2}-\frac{b}{\rho}\frac{\partial}{\partial y}\left(-\frac{\partial u}{\partial y}\right)^n-\frac{\sigma B_0^2}{\rho}u, \tag{2}$$

where a, b and n (≥ 0) are the material constants, σ the electrical conductivity of the fluid, ρ the fluid density, B_0 the magnitude of applied magnetic field.

The flow is subject to the following boundary conditions

$$u(x,y)=U=cx^s, v(x,y)=0 \text{ at } y=0, \tag{3}$$

$$u\to 0 \text{ as } y\to\infty, \tag{4}$$

where u and v are the velocity components along $x-$ and $y-$ directions, respectively.

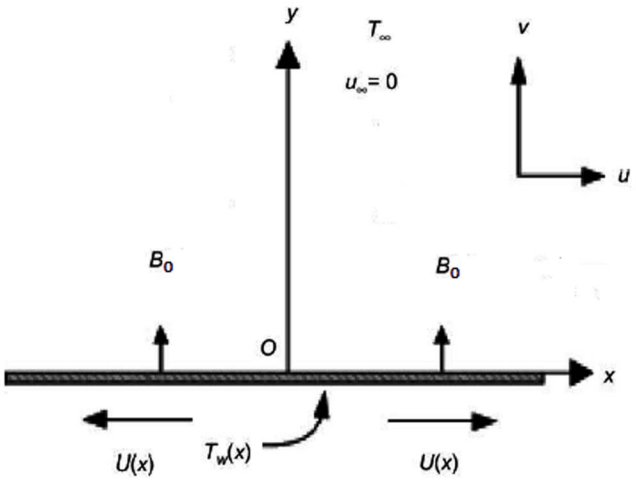

Figure 1. Schematic diagram of the problem.
doi:10.1371/journal.pone.0107989.g001

Introducing the transformations [20] as

$$\eta=\frac{y}{x}\mathrm{Re}_b^{\frac{1}{n+1}}, \psi=Ux\mathrm{Re}_b^{-\frac{1}{n+1}}f(\eta), \tag{5}$$

with

$$u(x,y)=Uf'(\eta), \tag{6}$$

$$v(x,y)=-U\mathrm{Re}_b^{-\frac{1}{n+1}}\frac{1}{n+1}[\{s(2n-1)+1\}f(\eta)+\{s(2-n)-1\}\eta f'(\eta)], \tag{7}$$

where ψ is the Stokes stream function.

After simplification we reach at the following problem [20]

$$Af'''+n(-f'')^{n-1}f'''+\frac{s(2n-1)+1}{n+1}ff''-s(f')^2-M^2f'=0, \tag{8}$$

Table 1. The convergence of the homotopy solutions when $n=2$, $s=1/2$, $M=A=\gamma=1$ and $\mathrm{Pr}=2$ are fixed.

Order of approximation	$-\frac{1}{2}\mathrm{Re}_b^{\frac{1}{n+1}}C_f$	$-\mathrm{Re}_b^{-\frac{1}{n+1}}Nu_x$
1	1.609750	0.463171
5	1.629799	0.448468
10	1.631518	0.451261
15	1.631523	0.450955
21	1.631523	0.450998
24	1.631523	0.450993
27	1.631523	0.450994
30	1.631523	0.450994

doi:10.1371/journal.pone.0107989.t001

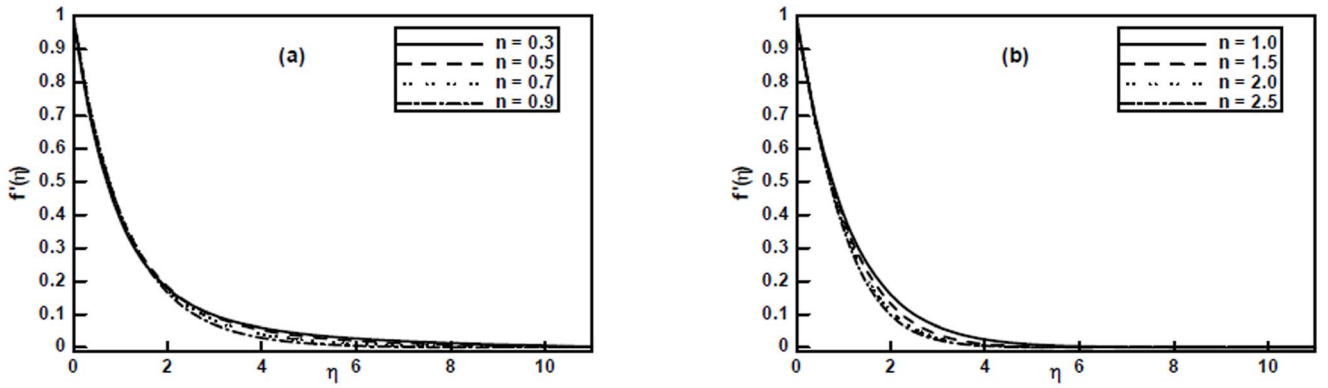

Figure 2. The velocity profiles $f'(\eta)$ for different values of the power-law index n when $s=A=1/2$, $M=1$ are fixed.
doi:10.1371/journal.pone.0107989.g002

$$f(0)=0, f'(0)=1, f'(\infty)=0, \tag{9}$$

where

$$M^2=\frac{\sigma B_0^2}{\rho U}x, A=\frac{\mathrm{Re}_b^{\frac{2}{n+1}}}{\mathrm{Re}_a}, \mathrm{Re}_a=\frac{\rho x U}{a} \text{ and } \mathrm{Re}_b=\frac{\rho x^n U^{2-n}}{b}, \tag{10}$$

are the non-dimensional quantities.

The significant quantity of interest is the skin-friction C_f given by [8]

$$\frac{1}{2}\mathrm{Re}_b^{\frac{1}{n+1}}C_f=Af''(0)-[-f''(0)]^n. \tag{11}$$

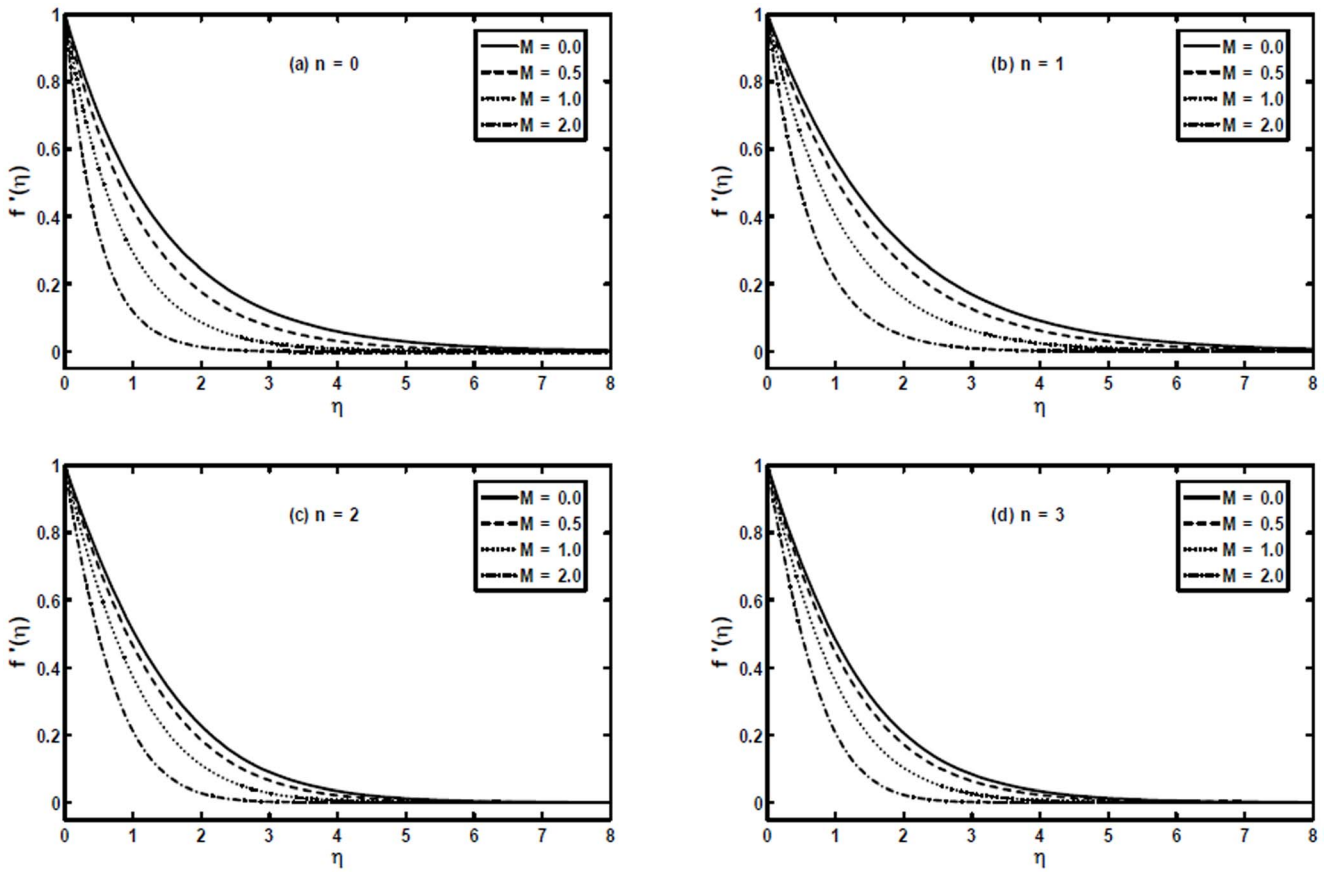

Figure 3. The velocity profiles $f'(\eta)$ for different values of the magnetic parameter M when $s=1/2$ and $A=1$ are fixed.
doi:10.1371/journal.pone.0107989.g003

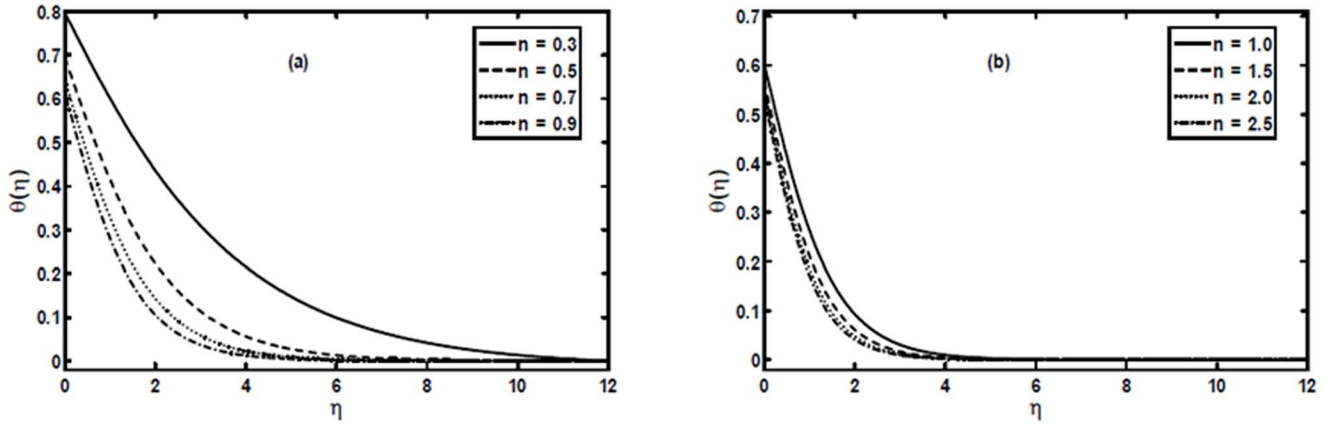

Figure 4. The temperature profiles $\theta(\eta)$ for different values of the power-law index n when $s=\mathrm{Pr}=1/2$, $A=\gamma=1$ and $M=1$ are fixed.
doi:10.1371/journal.pone.0107989.g004

Heat transfer analysis

The thermal energy equation after the application of usual thermal boundary layer approximation in the absence of heat source and dissipation with convective boundary condition at the wall is given as

$$u\frac{\partial T}{\partial x}+v\frac{\partial T}{\partial y}=\alpha\frac{\partial^2 T}{\partial y^2}, \tag{12}$$

$$k\frac{\partial T(x,0)}{\partial y}=-h_f\left[T_f-T(x,0)\right], \tag{13}$$

$$T\to T_\infty \text{ as } y\to\infty, \tag{14}$$

where $T=T(x,y)$ is the temperature field, k the thermal

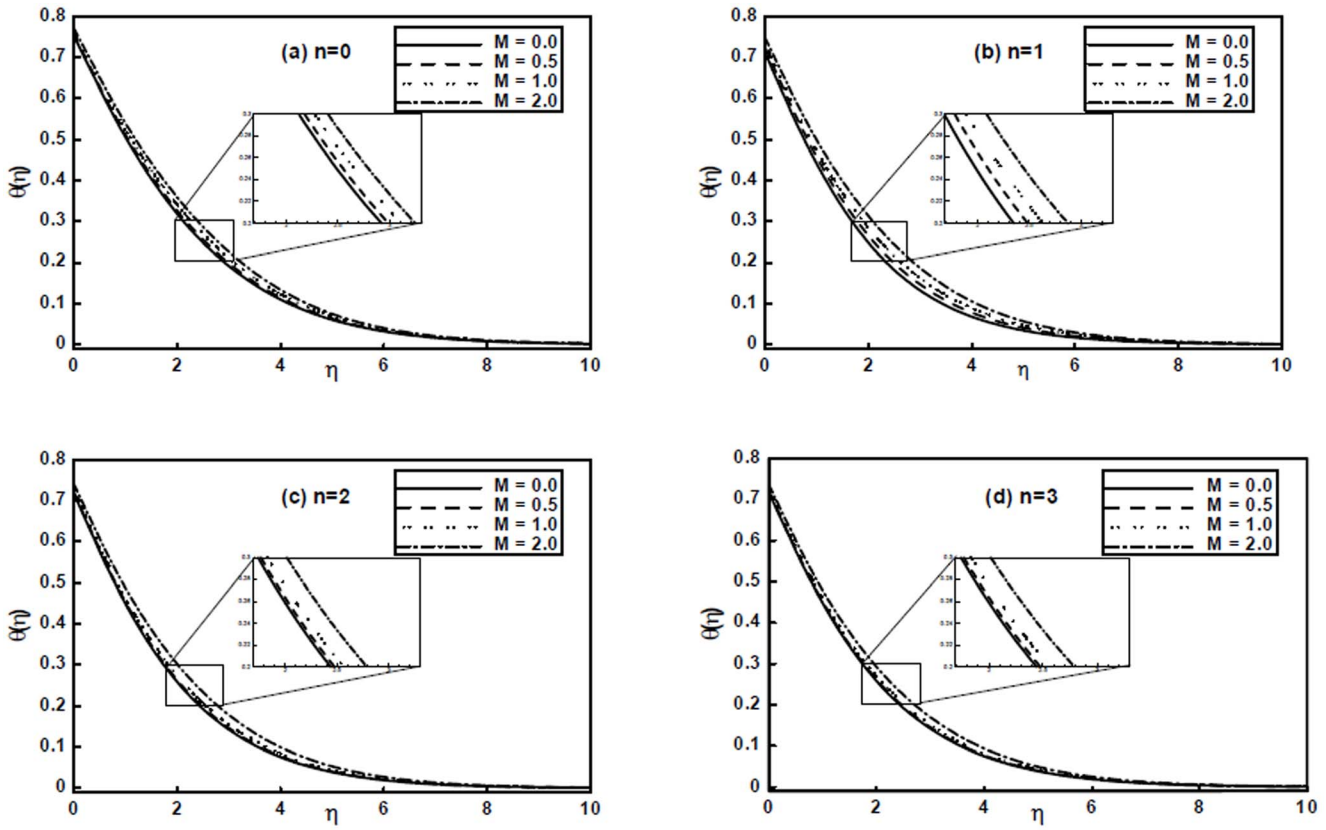

Figure 5. The temperature profiles $\theta(\eta)$ for different values of the magnetic parameter M when $s=\mathrm{Pr}=1/2$, $\gamma=1$ and $A=1$ are fixed.
doi:10.1371/journal.pone.0107989.g005

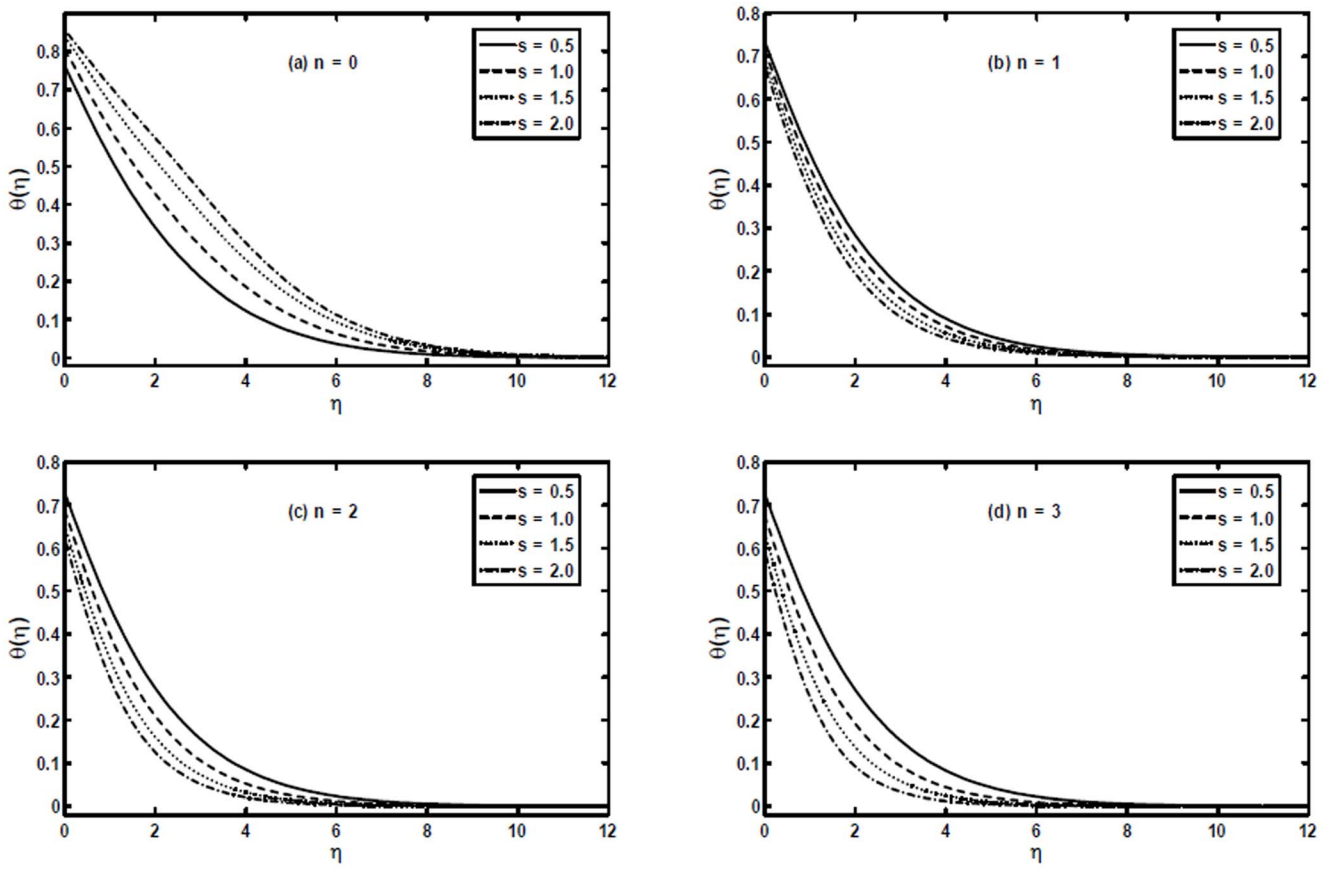

Figure 6. The temperature profiles $\theta(\eta)$ for different values of the stretching parameter s when $M=\gamma=1$, $\mathrm{Pr}=1/2$ and $A=1$ are fixed.
doi:10.1371/journal.pone.0107989.g006

conductivity, $\alpha=\frac{k}{\rho c_p}$ the thermal diffusivity, h_f the heat transfer parameter and T_∞ the ambient temperature of the fluid.

We introduce the non-dimensional scaled temperature θ as

$$\theta(\eta)=\frac{T-T_\infty}{T_f-T_\infty}. \tag{15}$$

Using Eqs. (5) and (15) Eq. (12) takes the form

$$\theta''+\frac{s(2n-1)+1}{n+1}\mathrm{Pr} f\theta'=0, \tag{16}$$

and transformed boundary conditions are

$$\theta'(0)=-\gamma[1-\theta(0)],\theta(\eta)\to 0 \text{ as } \eta\to\infty, \tag{17}$$

where prime denotes differentiation with respect to η, $\mathrm{Pr}=\frac{xU}{\alpha}\mathrm{Re}_b^{-\frac{2}{n+1}}$ the generalized Prandtl number and $\gamma=\frac{h_f}{k}x\mathrm{Re}_b^{-\frac{1}{n+1}}$ the generalized Biot number.

The local Nusselt number Nu_x may be found in terms of the dimensionless temperature at the wall surface, $\theta'(0)$, that is

$$\mathrm{Re}_b^{-\frac{1}{n+1}}Nu_x=-\theta'(0), \tag{18}$$

with $Nu_x=\frac{xq_w}{\kappa(T_f-T_\infty)}$ with q_w as the surface heat flux.

Solution Methodology

The homotopy analytic solution

The homotopy analysis method (HAM) is employed to solve non-linear Eqs. (8) and (16) subject to the boundary conditions (9) and (17) respectively. The analytic solutions are obtained for the velocity and temperature fields. The convergence of these solutions is ensured by taking the most suitable value of the auxiliary parameter $\hbar$ which is calculated using the squared residual error in each case of our calculations, where formula for squared residual error is given by [25]

$$E_{f,m}=\frac{1}{N+1}\sum_{j=0}^{N}\left[N_f\left(\sum_{i=0}^{m}f_j(i\Delta\eta)\right)\right]^2. \tag{19}$$

Table 1 elucidates the convergence of series solution. It shows that the convergence is achieved at 25th approximation in the mentioned case. Further, the same criteria are adopted to achieve the convergence in other cases.

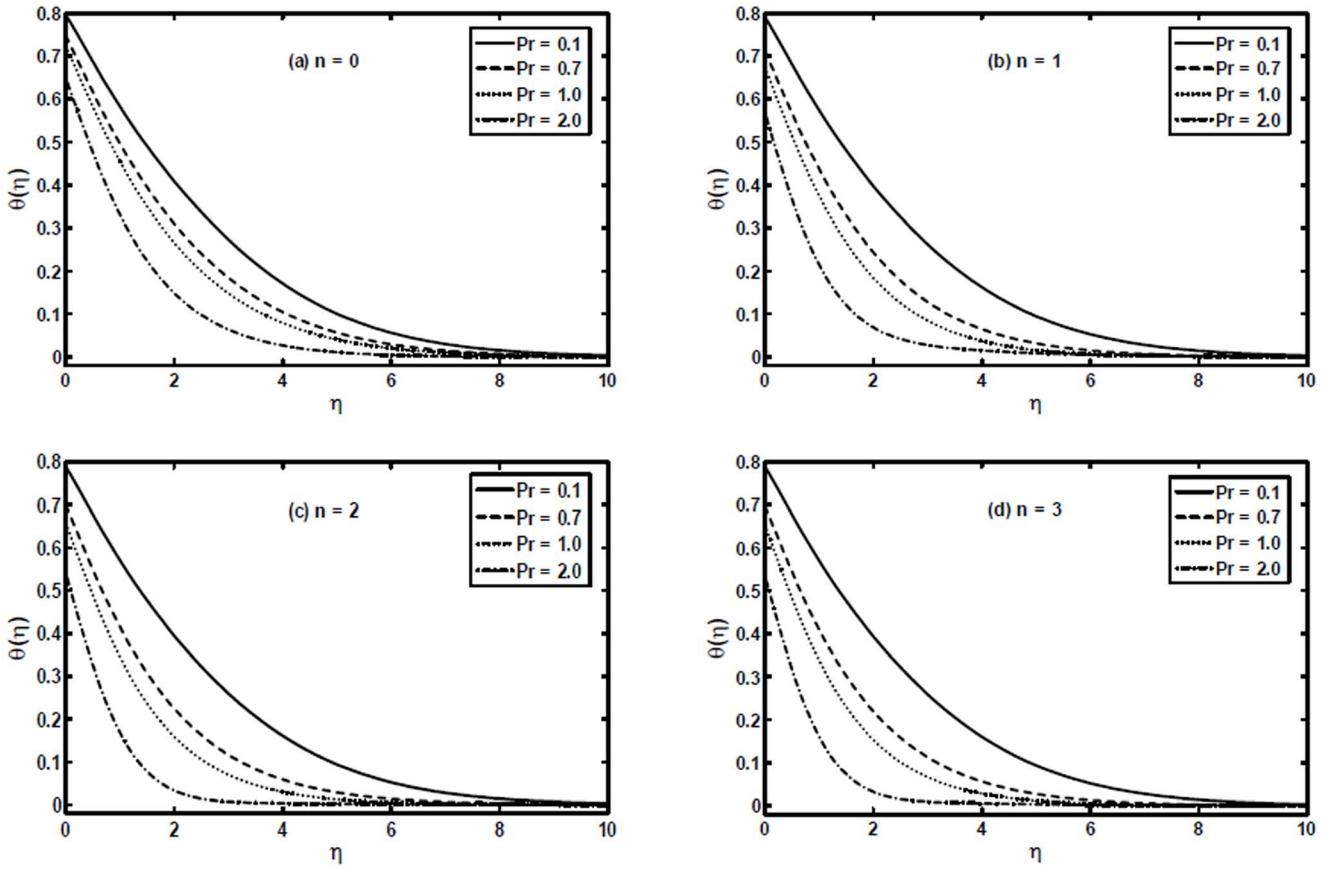

Figure 7. The temperature profiles $\theta(\eta)$ for different values of the generalized Prandtl number Pr when $s=1/2$, $M=\gamma=1$ and $A=1$ are fixed.
doi:10.1371/journal.pone.0107989.g007

Exact solutions for particular cases

Case (i). As a special case of the problem for $n=0$ and $s=1/2$ Eqs. (8) and (16) reduce to

$$2Af'''+ff''-(f')^2-2M^2f'=0, \tag{20}$$

and

$$\theta''+\frac{\Pr}{2}f\theta'=0. \tag{21}$$

The exact solutions of the above equations satisfying the boundary conditions (9) and (17) are (see ref. [20])

$$f(\eta)=\frac{1}{\beta}\left(1-e^{-\beta\eta}\right), \tag{22}$$

$$\theta(\eta)=\frac{2^{\frac{\Pr}{2\beta^2}}e^{\frac{\Pr}{2\beta^2}}\gamma\left[\Gamma\left(\frac{\Pr}{2\beta^2},0\right)-\Gamma\left(\frac{\Pr}{2\beta^2},\frac{\Pr}{2\beta^2}e^{-\beta\eta}\right)\right]}{\beta\left(\frac{\Pr}{\beta^2}\right)^{\frac{\Pr}{2\beta^2}}+2^{\frac{\Pr}{2\beta^2}}e^{\frac{\Pr}{2\beta^2}}\gamma\left[\Gamma\left(\frac{\Pr}{2\beta^2},0\right)-\Gamma\left(\frac{\Pr}{2\beta^2},\frac{\Pr}{2\beta^2}\right)\right]} \tag{23}$$

where $\beta=\sqrt{\frac{1+2M^2}{2A}}$ and $\Gamma(\cdot)$ the incomplete Gamma function.

Case (ii). Now for $n=1$ and $s=1$, Eqs. (8) and (16) become

$$(1+A)f'''+ff''-(f')^2-M^2f'=0, \tag{24}$$

and

$$\theta''+\Pr f\theta'=0, \tag{25}$$

which possess the exact analytical solutions of the form (see ref. [20])

$$f(\eta)=\frac{1}{\beta}\left(1-e^{-\beta\eta}\right), \tag{26}$$

$$\theta(\eta)=\frac{e^{\frac{\Pr}{\beta^2}}\gamma\left[\Gamma\left(\frac{\Pr}{\beta^2},0\right)-\Gamma\left(\frac{\Pr}{\beta^2},\frac{\Pr}{\beta^2}e^{-\beta\eta}\right)\right]}{\beta\left(\frac{\Pr}{\beta^2}\right)^{\frac{\Pr}{\beta^2}}+e^{\frac{\Pr}{\beta^2}}\gamma\left[\Gamma\left(\frac{\Pr}{\beta^2},0\right)-\Gamma\left(\frac{\Pr}{\beta^2},\frac{\Pr}{\beta^2}\right)\right]}, \tag{27}$$

with $\beta=\sqrt{\frac{1+M^2}{1+A}}$.

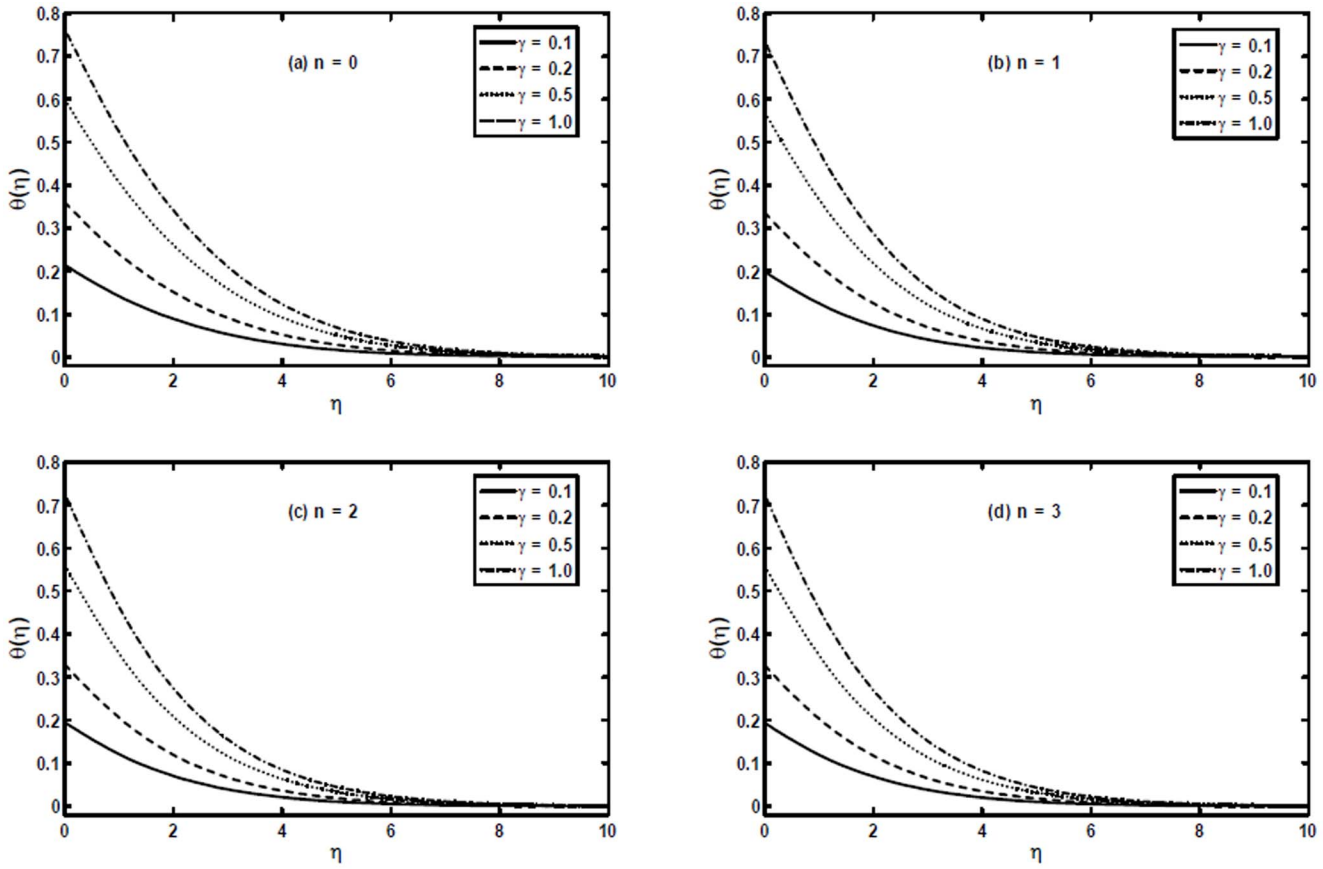

Figure 8. The temperature profiles $\theta(\eta)$ for different values of the generalized Biot number γ when $s=\mathrm{Pr}=1/2$, $M=1$ and $A=1$.
doi:10.1371/journal.pone.0107989.g008

Numerical Results and Discussion

In order to get definite perception of the physical problem, velocity profile $f'(\eta)$ and temperature profile $\theta(\eta)$ are displayed graphically for different values of the power-law index n,magnetic parameter M, stretching parameter s, generalized Prandtl number Pr and generalized Biot number γ appearing in the problem. The coupled set of Eqs. (8) and (16) with the boundary conditions (9) and (17) are solved analytically by means of the HAM and numerical solutions are obtained using the shooting method. Further, it is possible in some special cases to compare the results obtained by the HAM with exact solutions. Moreover, representative results for the skin-friction coefficient and local Nusselt number illustrating the influence of various physical parameters of the flow are recorded through tables.

Taking into account the obtained numerical solutions, figures 2(a, b) delineate the influence of the non-integer power-law index n on velocity profile $f'(\eta)$. From these figures, it is observed

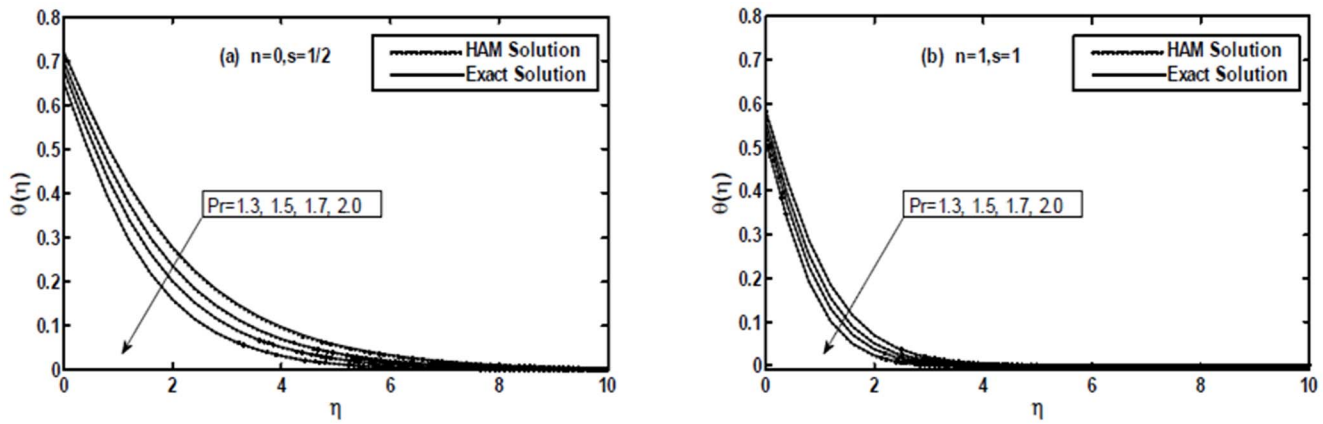

Figure 9. The comparison of the HAM solution with exact solution for the temperature profile $\theta(\eta)$ when $M=A=1/2$ and $\gamma=1$ are fixed.
doi:10.1371/journal.pone.0107989.g009

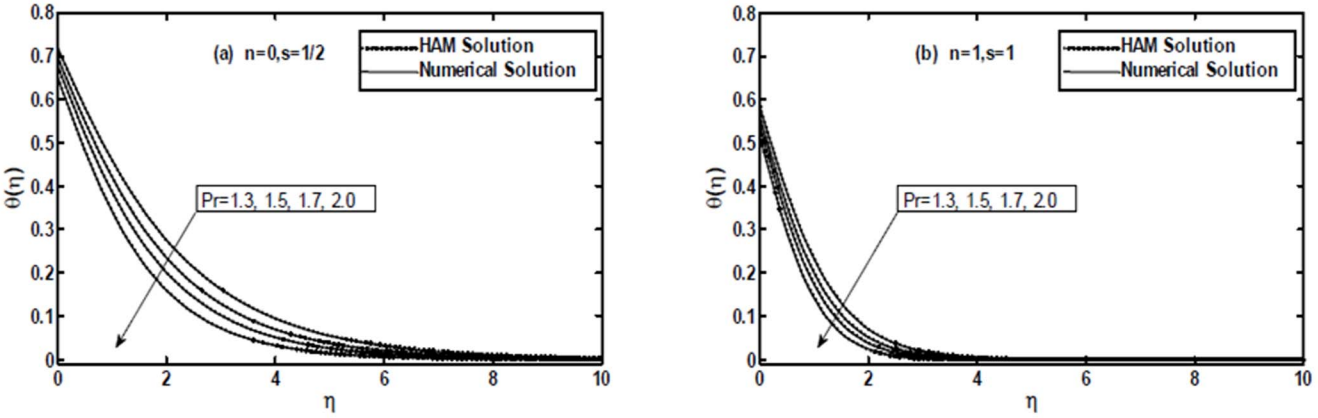

Figure 10. The comparison of the HAM solution with numerical solution for the temperature profile $\theta(\eta)$ when $M = A = 1/2$ and $\gamma = 1$ are fixed.
doi:10.1371/journal.pone.0107989.g010

that an increase in the values of n decreases the velocity profile and hence the boundary layer thickness for power index $n \geq 1$ whereas for $n < 1$ we notice two different behaviors, i.e., close to the sheet the velocity profile increases while it decreases away from the sheet with the increase of the power-law index n.

In order to illustrate the influence of the magnetic parameter M on velocity profile $f'(\eta)$ we have plotted figures 3(a-d) for the power-law index $n = 0, 1, 2$ and 3. It appears from these figures that an increase in value of the magnetic parameter M decreases the velocity profile due to resistance force generated by the magnetic field. Also, we can notice that effect of the magnetic parameter M becomes less dominating as we increase value of the power-law index n and boundary layer thickness decreases with the increase of M too. Further, these figures portray that the boundary layer thickness becomes thin as we decrease the power-law index n. Moreover, these figures provide a comparison that the magnitude of velocity is larger for hydrodynamic case ($M = 0$) when compared with hydromagnetic case ($M \neq 0$).

Figures 4(a, b) correspond to the numerical solution obtained for the non-integer power-law index $n < 1$ and $n \geq 1$, respectively. From these figures, it is obvious that the temperature profile decreases with increase in the power-law index n. Further, these figures indicate that for a given location η, $\theta(\eta)$ decreases as the power-law index n increases, resulting in a decrease of the thermal boundary layer thickness. We can also observe that more significant effects can be seen for values of the power-law index $n < 1$, while it has small effects for the power-law index $n \geq 1$.

Figures 5(a–d) portray the effects of the magnetic parameter M on temperature profile $\theta(\eta)$. It is clear from these figures that the temperature profile increases with an increase of M. However, we can observe that the temperature profile is not very much sensitive to the magnetic parameter M.

Figures 6(a–d) present the temperature profile $\theta(\eta)$ for different values of the stretching parameter s. We can notice from these figures that the stretching parameter has quite opposite effect on the temperature profile for $n = 0$ and $n = 1, 2, 3$. We can see that with an increase in the stretching parameter s the temperature

Table 2. Numerical values of the skin friction coefficient $\frac{1}{2}\mathrm{Re}_b^{\frac{1}{n+1}} C_f$ for different values of physical parameters.

A	M	s	$-\frac{1}{2}\mathrm{Re}_b^{\frac{1}{n+1}} C_f$			
			$n=0$	$n=1$	$n=2$	$n=3$
0.0	1.0	0.5	1.000000	1.259683	1.168175	1.121380
1.0			2.224745	1.781461	1.631523	1.558845
2.0			2.732051	2.181835	2.024553	1.954535
3.0			3.121320	2.519366	2.366378	2.304718
1.0	0.0		1.707107	1.089465	0.962186	0.908237
	0.5		1.866025	1.296307	1.153318	1.090619
	1.0		2.224745	1.781461	1.631523	1.558845
	2.0		3.121320	3.028033	2.999168	2.981083
	1.0	0.5	2.224745	1.781461	1.631523	1.558845
		1.0	2.290994	2.00000	1.914495	1.875081
		2.0	2.431934	2.376857	2.412204	2.446648
		3.0	2.573536	2.701216	2.851608	2.965925

doi:10.1371/journal.pone.0107989.t002

Table 3. Numerical values of the local Nusselt number $\mathrm{Re}_b^{-\frac{1}{n+1}} Nu_x$ for different values of physical parameters.

A	M	Pr	γ	s	$-\mathrm{Re}_b^{-\frac{1}{n+1}} Nu_x$			
					$n=0$	$n=1$	$n=2$	$n=3$
1.0	1.0	0.0	1.0	0.5	0.240458	0.331260	0.340045	0.342428
2.0					0.275129	0.346666	0.357093	0.360945
3.0					0.291544	0.355742	0.367068	0.371748
1.0	0.0				0.291544	0.362207	0.367377	0.368707
	0.5				0.275129	0.353119	0.359256	0.360679
	1.0				0.240458	0.331260	0.340045	0.342428
	1.0	0.7			0.191051	0.277793	0.284027	0.285370
		1.0			0.240458	0.353119	0.340045	0.342428
		2.0			0.349286	0.438483	0.450994	0.455287
		1.0	0.1		0.075993	0.083203	0.083747	0.083891
			0.5		0.193846	0.248832	0.253757	0.255081
			1.0		0.240458	0.331260	0.340045	0.342428
			1.0	0.5	0.240458	0.331260	0.340045	0.342428
				0.7	0.173867	0.347092	0.370199	0.378838
				1.0	0.024606	0.367879	0.406270	0.420928

doi:10.1371/journal.pone.0107989.t003

profile increases for $n=0$, while for $n=1, 2, 3$ it decreases. Further, with the increase in s the thermal boundary layer thickness increases for $n=0$ and decreases for $n=1, 2, 3$.

The variation of the generalized Prandtl number $\mathbf{Pr}$ on the temperature profile $\theta(\eta)$ is shown in Figures 7(a–d). It is worth noting that with the increase of $\mathbf{Pr}$ the temperature profile decreases. That is, an increase in generalized Prandtl number $\mathbf{Pr}$ results in a decrease in the thermal conductivity which as a result reduces the thermal boundary layer thickness. Additionally, it can be observed that the power-law index n plays a significant role. An increase in the power-law index n results in thinning of the thermal boundary layer.

Figures 8(a–d) show the effect of the generalized Biot number γ on the temperature profile $\theta(\eta)$. These figures put in evidence that the effect of increasing the generalized Biot number γ is to enhance both the temperature and thermal boundary layer thickness significantly. It is due to the fact increasing values of γ shows the decreasing thermal resistance of the wall and hence convective heat transfer to the fluid increases.

Figures 9(a, b) and 10(a, b) present a comparison between the exact, numerical and HAM solutions. These figures show that excellent agreement between the results exists. This leads confidence in the HAM results reported in this section.

The numerical values of the skin friction coefficient $\frac{1}{2}\mathrm{Re}_b^{\frac{1}{n+1}} C_f$ and local Nusselt number $\mathrm{Re}_b^{-\frac{1}{n+1}} Nu_x$ for different values of A, M, s, Pr and γ are listed in tables 2 and 3. Table 2 shows that magnitude of the skin friction coefficient increases for larger values of A, M and s. Table 3 depicts that the local Nusselt number increases for larger values of A, Pr, γ while it has opposite behavior for M for different values of the power-law index n. By increasing the stretching parameter s we observe that for $n=0$, the local Nusselt number decreases while for $n=1, 2$ and 3 it increases.

Conclusions

In this study, we have investigated the heat transfer with convective boundary condition at the wall for Sisko fluid flow over a non-linearly stretching sheet in the presence of a transverse uniform magnetic field. The governing non-linear equations were formulated and solved analytically by the HAM and numerically by shooting method. Additionally, the exact analytical solutions have been determined for the power-law index $n=0$ and $n=1$. The obtained results imply the following pronouncements.

- For the power-law index $n=1, 2, 3$ the velocity profile as well as boundary layer thickness was decreased for stretching parameter s whereas, for $n=0$ boundary layer thickness was increased.
- Behavior of the material parameter A and magnetic parameter M on velocity profile were quite opposite.
- Behavior of stretching parameter s for the temperature profile was similar to that of velocity profile qualitatively.
- The influence of Pr, and n was to decrease the temperature field $\theta(\eta)$ and hence decreased the thermal boundary layer while it increased for M and γ.
- For the increasing power-law index n velocity profile as well as temperature profile was decreased and these effects were more noticeable when considering $n<1$ as compared to $n\geq 1$

It is expected that the present analysis serves as stimulus for the shear thinning and thickening fluid flows in the areas where high rate of heat transfer or rate of cooling is required such as extrusion processes, glass fiber and storage of thermal energy.

Author Contributions

Conceived and designed the experiments: RM MK AM WAK. Performed the experiments: RM MK AM WAK. Analyzed the data: RM MK AM WAK. Contributed reagents/materials/analysis tools: RM MK AM WAK. Wrote the paper: RM MK AM WAK.

References

1. Ibrahim W, Shankar B, Nandeppanavar MM (2013) MHD stagnation point flow and heat transfer due to nanofluid towards a stretching sheet. Int J Heat Mass Transf 56 (1-2) 1–9.
2. Sarif NM, Salleh MZ, Nazar R (2013) Numerical solution of flow and heat transfer over a stretching sheet with Newtonian heating using the Keller box method. Procedia Eng 53 542–554.
3. Hayat T, Shafiq A, Alsaedi A, Awais M (2013) MHD axisymmetric flow of third grade fluid between stretching sheets with heat transfer. Comput Fluids 86 103–108.
4. Bhattacharyya K (2013) Heat transfer analysis in unsteady boundary layer stagnation-point flow towards a shrinking/stretching sheet. Ain Shams Eng J 4 (2) 259–264.
5. Hayat T, Farooq M, Alsaedi A, Iqbal Z (2012) Mixed convection Falkner-Skan flow of a Maxwell fluid. J Heat Transf 134 114504.
6. Arnold JC, Asir AA, Somasundaram S, Christopher T (2010) Heat transfer in a viscoelastic boundary layer flow over a stretching sheet. Int J Heat Mass Transf 53 (5-6) 1112–1118.
7. Cortell R (2014) Fluid flow and radiative nonlinear heat transfer over a stretching sheet. J King Saud University- Science 26 (2) 161–167.
8. Hakeem AKA, Kalaivanan R, Ganesh NV, Ganga B (2014) Effect of partial slip on hydromagnetic flow over a porous stretching sheet with non-uniform heat source/sink, thermal radiation and wall mass transfer. Ain Shams Eng J Available: http://dx.doi.org/10.1016/j.asej.2014.02.006.
9. Bachok N, Ishak A, Pop I (2012) Boundary layer stagnation-point flow and heat transfer over an exponentially stretching/shrinking sheet in a nanofluid. Int J Heat Mass Transf 55 (25-26) 8122–8128.
10. Nandeppanavar MM, Vajravelu K, Abel MS, Ng C (2011) Heat transfer over a nonlinearly stretching sheet with non-uniform heat source and variable wall temperature. Int J Heat Mass Transf 54 (23-24) 4960–4965.
11. Bataller RC (2008) Radiation effects for the Blasius and Sakiadis flow with a convective surface boundary conditions. Appl Math Comput 206 832–840.
12. Yao S, Fang T, Zhong Y (2011) Heat transfer of a generalized stretching/shrinking wall problem with convective boundary conditions. Commun Nonlinear Sci Numer Simulat 2 752–760.
13. Hammad MAA, Uddin MJ, Ismail AIM (2012) Radiation effects on heat and mass transfer in MHD stagnation-point flow over a permeable flat plate with thermal convective surface boundary condition. Nuclear Eng Design 242 194–200.
14. Vajravelu K, Prasad KV, Ng C (2013) Unsteady convective boundary layer flow of a viscous fluid at a vertical surface with variable fluid properties. Nonlinear Anal: Real World Appl 14 (1) 455–464.
15. Shahzad SA, Alsaedi A, Hayat T (2012) Three-dimensional flow of Jeffery fluid with convective surface boundary conditions. Int J Heat Mass Transf 55 (15-16) 3971–3976.
16. Hayat T, Iqbal Z, Mustafa M, Alsaedi A (2012) Momentum and heat transfer of an upper-convected Maxwell fluid over a moving surface with convective boundary conditions. Nuclear Eng Design 252 242–247.
17. Hayat T, Iqbal Z, Qasim M, Obaidat S (2012) Steady flow of an Eyring Powell fluid over a moving surface with convective boundary conditions. Int J Heat Mass Transf 55 1817–1822.
18. Srinivas S, Malathy T, Reddy AS (2014) A note on thermal-diffusion and chemical reaction effects on MHD pulsating flow in a porous channel with slip and convective boundary conditions. J King Saud University-Engineering Sciences Available: http://dx.doi.org/10.1016/j.jksues.2014.03.011.
19. Makinde OD (2009) Thermal stability of a reactive viscous flow through a porous-saturated channel with convective boundary conditions. Appl Thermal Eng 29 (8-9) 1773–1777.
20. Khan M, Shahzad A (2012) On boundary layer flow of a Sisko fluid over a stretching sheet. Quaestiones Mathematicae 36 137–151.

21. Molati M, Hayat T, Mahomed F (2009) Rayleigh problem for a MHD Sisko fluid. Nonlinear Anal: Real World Appl 10 3428–3434.
22. Khan M, Farooq J (2010) On heat transfer analysis of a magnetohydrodynamic Sisko fluid through a porous medium. J Porous Med 13 (3) 287–294.
23. Khan M, Munawa S, Abbasbandy S (2010) Steady flow and heat transfer of a Sisko fluid in annular pipe. Int J Heat Mass Transf 53 1290–1297.
24. Khan M, Shaheen N, Shahzad A (2012) Steady flow and heat transfer of a MHD Sisko fluid through porous medium in annular pipe. Int J Numer Methods Fluids 69 1907–1922.
25. Liao S (2012) Homotopy Analysis Method in Nonlinear Differential Equations. Springer London.